

An Improved Inherent Optical Properties Data Processing System for Residual Error Correction in Turbid Natural Waters

Jun Chen ^{1b}, Wenting Quan, Hongtao Duan ^{1b}, Qianguo Xing, and Na Xu ^{1b}

Abstract—Being able to accurately estimate inherent optical properties (IOPs) at long time scales is key to comprehending the aquatic biological and biogeochemical responses to long-term global climate change. We employed the near-infrared band and combined it with four “common bands” at visible wavelengths (around 443, 490, 551, and 670 nm) to adjust the IOPs data processing system, IDAS_{v2}. We applied the IDAS_{v2} algorithm further to correct for the residual error in images of turbid waters. We evaluated the performance of the IDAS_{v2} algorithm using datasets covering a wide range of natural water types from clear open ocean to turbid coastal and inland waters. Due to the water-leaving signals’ sensitivity to the optically significant constituents of highly turbid waters, the near-infrared band was very important for retrieving IOPs from those waters. In our analysis, we found that the IDAS_{v2} algorithm provided IOPs data with <28.36% uncertainty for oceanic waters and <37.83% uncertainty for inland waters, which was much more effective than what a quasi-analytical algorithm provided. Moreover, the near-infrared band was better at removing the residual error and partial intermission bias in satellite remote sensing reflectance (R_{rs}) data because of the strong absorption of pure water. We tested the IDAS_{v2} algorithm with numerically simulated and satellite observed data of turbid water. After applying IDAS_{v2}, the IOPs data were accurately determined from R_{rs} data contaminated by the residual error. Furthermore, the mean intermission difference between Medium Resolution Spectral Imager 2 and Visible Infrared Imaging Radiometer R_{rs} data at 443 and 551 nm decreased from 8%–25% to 1%–9%. These results suggest that we can accurately estimate IOPs data for natural waters including naturally clear and turbid waters.

Index Terms—IDAS, inherent optical property, natural turbid water.

I. INTRODUCTION

OCEANIC color remote sensing initially focused on estimating the chlorophyll-a concentration in the upper ocean at basin and global scales [1], [2]. This narrow view focused on using chlorophyll-a products to indicate plankton biomass, to input chlorophyll-a concentration into primary production models, or to trace oceanographic plumes [3]. However, ocean scientists in the 1980s began to realize that sensors in space were not simply interesting novelties but were essential for developing their research at a global scale [4]. Water color is determined by inherent optical properties (IOPs) like the absorption coefficient (a) and backscattering coefficient (b_b), and chlorophyll is just one of the optically significant constituents that influences the IOPs of a water body [5]. Ocean color satellites can and should generate more bio-optical products than just chlorophyll pigment concentration. The absorption and backscattering coefficients are directly associated with optically significant constituents in the water column [6], [7], and can be used to determine the type of water [8], [9], subsurface light intensity [10]–[12], phytoplankton community composition [13], [14], carbon cycles [15], [16], and so on [5]. At present, absorption and backscattering coefficient data are widely used to assess the health of aquatic ecosystems.

Many IOPs processing systems include empirical, quasi-analytical, or semianalytical algorithms and were established over the past several decades [16]–[19]. These algorithms effectively process satellite data when the satellites’ spectral bands are similar to the algorithms’ requirements. However, some problems can arise when the spectral bands do not agree well with the algorithms’ inputs. For example, when applying the algorithms proposed by Garver and Siegel [17] and Smyth *et al.* [19], modifications are needed to quantify the absorption coefficients from Moderate Resolution Imaging Spectroradiometer (MODIS) and visible infrared imaging radiometer (VIIRS) data because these sensors do not have the spectral band at 510 nm that the Garver and Siegel algorithms require. As a result, for practical applications we always have to adjust the retrieval procedures according to the satellites’ spectral characteristics. In addition, it is well known that different algorithms always respond differently to the residual errors and intermission bias in

Manuscript received November 13, 2020; revised March 9, 2021; accepted April 7, 2021. Date of publication April 14, 2021; date of current version July 14, 2021. This work was supported in part by the National Key R&D Program of China under Grant 2018YFB0504802, in part by the National Natural Science Foundation of China under Grant 42022045, and in part by the International Cooperation in Science and Technology Innovation among Governments under Grant SQ2019YFE012389. (Corresponding authors: Jun Chen and Na Xu.)

Jun Chen is with the State Key Laboratory of Satellite Ocean Environment Dynamics, Second Institute of Oceanography, Ministry of Natural Resources, Hangzhou 310012, China, and also with the School of Human Settlements and Civil Engineering, Xi’an Jiaotong University, Xi’an 710049, China (e-mail: chenjun@xjtu.edu.cn).

Wenting Quan is with the Meteorological Service Center of Agricultural Remote Sensing and Economic Crop, Xi’an 71000, China (e-mail: quanwenting@163.com).

Hongtao Duan is with the Key Laboratory of Watershed Geographic Sciences, Nanjing Institute of Geography and Limnology, Chinese Academy of Sciences, Nanjing 210008, China (e-mail: htduan@niglas.ac.cn).

Qianguo Xing is with the Yantai Institute of Coastal Zone Research, Chinese Academy of Sciences, Yantai 264003, China (e-mail: xingqg@163.com).

Na Xu is with the National Satellite Meteorological Centre, China Meteorological Administration, Beijing 100081, China (e-mail: xuna@cma.gov.cn).

Digital Object Identifier 10.1109/JSTARS.2021.3073168

satellite data [20], which can cause inconsistent outputs among the different algorithms even for the same water-leaving signals [21]. This is a disadvantage for generating smooth and long-term series of IOPs data on global or local scales.

Second-generation satellites have four “common bands” around 443, 490, 551, and 670 nm at visible wavelengths. By using the remote sensing reflectance (R_{rs}) in these four “common bands” as inputs, a quasi-analytical algorithm (QAA) [18] and an IOP data processing system (Version 1, abbreviated to IDAS_{v1}) [21] can estimate the IOPs from any visible band as long as the R_{rs} for this visible band is known. For most of the open ocean, because $R_{rs}(551)$ and $R_{rs}(670)$ are relatively stable, and $R_{rs}(443)$ and $R_{rs}(490)$ are sensitive to phytoplankton and covarying optically significant constituents [22], it is possible to effectively derive IOPs from R_{rs} at these four “common bands.” However, if the water is turbid, like some coastal water, optically significant constituents absorb so much light that there is little radiance escaping at blue bands [23]. Having such small amounts of radiance escaping from turbid water means that small variations in the IOPs might lead to the covarying magnitude of R_{rs} being ignored at the blue bands. For example, Doxaran *et al.* [24] and Han *et al.* [25] showed that the R_{rs} values at visible bands tend to saturate because of the suspended particulate in highly turbid water. Thus, it is questionable whether the four “common bands” can offer sufficient optical information for estimating the IOPs of highly turbid water. Fortunately, there is sufficient scattering that overcomes the strong absorption at near-infrared wavelengths, so the near-infrared wavelengths should be combined with the “common bands” to retrieve IOPs from highly turbid water.

For a perfectly calibrated instrument, where the top-of-atmospheric radiance or reflectance is error free, imperfect atmospheric correction is the main source of error in the satellite-derived R_{rs} . Considering all potential error sources in the atmospheric correction, Chen *et al.* [20] showed that there are 4.70% and 12.04% uncertainties in SeaWiFS Level-2 global area coverage (GAC) $R_{rs}(443)$ and $R_{rs}(555)$ data for the open ocean, respectively. The uncertainties for turbid waters are much larger than for the open ocean [23], [26]. In the QAA algorithm, because the R_{rs} data contained substantial uncertainties, when a at reference wavelength (λ_0) is “fixed” with high accuracy, the uncertainties in $R_{rs}(\lambda_0)$ propagates to $b_b(\lambda_0)$ following the IOPs– R_{rs} relationship [27]. Thus, it is impossible to simultaneously obtain highly accurate absorption and backscattering coefficients from satellite R_{rs} that is contaminated with errors using the QAA or IDAS_{v1} algorithms unless the uncertainties are removed by correcting for the residual error [21]. Furthermore, to accurately derive absorption and backscattering coefficients, it is necessary to reconstruct the method of the QAA or IDAS_{v1} algorithm.

Neural network models would be good candidate methods for retrieving absorption and backscattering coefficients from satellite or field R_{rs} data, if we can assimilate some spectral properties of the residual error into the neural network procedures. Using 443, 490, 551, 670, and 865 nm as five “common bands,” in this study, we updated the IDAS_{v1} algorithm, used to retrieve IOPs from natural waters, and we renamed it IDAS version 2 (IDAS_{v2}). Our specific goals were as follows:

TABLE I
RANGE OF OPTICAL PROPERTIES OF THE SYNTHETIC DATASET, OCEANIC DATASET, LAKE DATASET, AND MATCHUP DATASET USED FOR TO INITIALIZE AND EVALUATE THE MODEL

Data	IOPs	Min	Max	Median	Average	STD
Synthetic data set ($n=90,000$)	$a(551)$	0.0599	71.5097	0.1340	2.8079	6.8380
	$b_b(670)$	0.0004	35.5824	0.0376	1.3484	4.1266
	Y	-	2.8828	0.6892	0.7186	0.6796
Oceanic data set ($n=1,590$)	$a(551)$	0.0597	26.0632	0.1685	0.6829	1.9478
	$b_b(670)$	0.0004	5.2761	0.0239	0.1539	0.6542
	Y	-	2.3783	0.8372	0.9040	0.4814
Lake data set ($n=338$)	$a(551)$	0.0802	8.0001	1.1062	1.5756	1.4622
	$b_b(670)$	0.0024	3.4266	0.4078	0.5854	0.5681
	Y	-	2.7739	1.1141	1.6338	1.5778
Matchup data set ($n=847$)	$a(551)$	0.0598	1.2657	0.0789	0.1008	0.0769
	$b_b(670)$	0.0006	0.5925	0.0029	0.0119	0.0476
	Y	0.0009	2.1524	0.9260	0.9896	0.5983

STD represents the standard derivation, while Y represents the power coefficient of the particle backscattering coefficients.

- 1) to improve the IDAS_{v1} algorithm with neural network technology so that we could estimate absorption and backscattering coefficients at near-infrared bands;
- 2) to test the accuracy and stability of the new IDAS_{v2} algorithm at predicting the absorption and backscattering coefficients using field measurements collected from natural waters;
- 3) to compare the performance of the IDAS_{v2} algorithm with the QAA algorithm for water with widely varying optical properties; and
- 4) to analyze how well the IDAS_{v2} algorithm corrects the intermission consistency in data of turbid water.

II. DATA AND METHODS

A. Data Used

We used synthetic data, *in situ* data, matchup data, and satellite data to train the IDAS_{v2} algorithm and test how well it retrieves the absorption and backscattering coefficients and corrects for the residual error.

1) *Synthetic Dataset*: While we trained our model and tested our procedures, we were limited by the availability of adequate datasets because individual groups measured data from limited regions, which made it difficult to assess how well the algorithms performed at broader scales [5]. To overcome these data limits, we generated a large synthetic dataset (see Table I) using Hydrolight, which we used to train the IDAS algorithm. This dataset had 443, 490, 551, 670, and 865 nm bands that contained 90,000 data points with chlorophyll-a kept randomly fixed from 0.003 to 80 $\mu\text{g l}^{-1}$. We kept mineral material randomly fixed from 0.006 to 1600 mg l^{-1} , and we kept the gelbstoff absorption coefficient at 443 nm randomly fixed from 0.001 to 10 m^{-1} . All these parameter ranges followed the default “Case 2” model that is included in Hydrolight 5.2 [28]. Furthermore, we generated another 6029 data points with Hydrolight to test if IDAS_{v2} could be applied to correct for residual errors in turbid waters. The Hydrolight-simulated data can be considered error-free data,

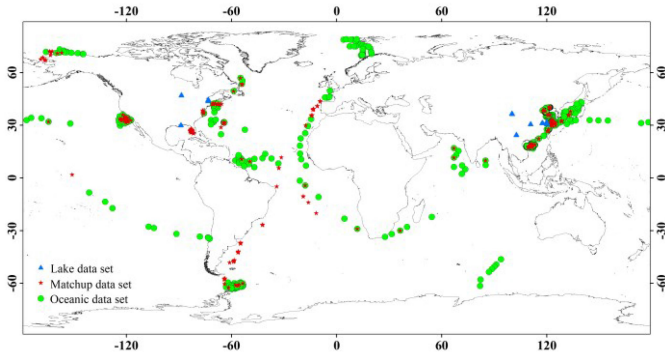


Fig. 1. Locations of field measurements. The blue triangle, red star, and green circle represent Lake, matchup, and oceanic data sets, respectively.

noting that the R_{rs} data usually contain substantial uncertainty. To keep consistent data quality with the R_{rs} data, we used a numerical approach proposed by Chen *et al.* [20] to simulate the residual error in R_{rs} and added these simulated residual errors to the Hydrolight-simulated R_{rs} data.

2) *Field Measurements*: We collected three field datasets to evaluate the accuracy and stability of IOP retrieval algorithms for oceanic and inland lake waters (see Table I and Fig. 1).

The first dataset was a global set of field measurements archived by the National Aeronautics and Space Administration (NASA) SeaWiFS Project, known as the NASA Optical Marine Algorithm Dataset (NOMAD). However, there were no $R_{rs}(865)$ data in the NOMAD dataset. To overcome this problem, for each point, we calculated $b_b(865)$ using a b_b spectral model determined from field-measured IOPs data, and then we estimated $R_{rs}(865)$ using the IOPs- R_{rs} relationship that Bailey *et al.* [29] developed. We augmented the NOMAD data with 218 data points from the Yellow and the China Eastern Seas, 182 data points from the Bohai Sea, 53 data points from the Hangzhou Bay, 76 data points from the Oujiang River Estuary, and 74 data points from the South Chinese Sea, and we called the augmented data the oceanic dataset.

For our second dataset, we collected 187 data points from the Taihu Lake, 30 data points from the Chaohu Lake, 25 data points from the Dianchi Lake, 13 data points from the Qinghai Lake, 25 data points from the Three Gorges Reservoir, and 58 data points from lakes in the United States, and we called these data the lake dataset. Note that these data were rigorously measured following the community-defined protocols for experiment deployment and data collection that Mueller *et al.* [30] outlined.

Finally, we collected a matchup dataset from the SeaWiFS Bio-optical Archive and Storage System to evaluate how accurate the IDAS algorithm is at deriving absorption and backscattering coefficients from satellite R_{rs} . These matchup data were field-measured IOPs versus satellite R_{rs} , but there was no $R_{rs}(865)$ in this matchup dataset. We implemented the same procedure that we used for the NOMAD dataset to estimate $R_{rs}(865)$ and add it to the matchup data. In addition, we added 26 data points from the South China Sea, 27 data points from the Yellow Sea and the East China Sea, 27 data points from the Bohai Sea, and 10 data points from the Oujiang River Estuary.

We used the SeaBASS default exclusion criteria that Bailey and Werdell [31] proposed to discard any “low-quality” data from the matchup data.

3) *Satellite Data*: The Medium Resolution Spectral Imager 2 (MERSI2) is the second generation of China’s polar orbiting meteorological and oceanographic instruments. The satellite was launched on 15 November 2017. To test how well the IDAS_{v2} algorithm removed the residual error and provided consistent intermission IOPs data from turbid water, we collected three VIIRS and MERSI2 image pairs on 17 April 2018 from the Eastern China Coastal Seas. We stitched together those three images to make one big image that covered the entire Eastern China Coastal Seas. Because there were many uncertainties in the original calibration coefficients of the MERSI2 data, we used the cross-calibration model that Chen *et al.* [32] developed to improve the data quality of the MERSI2 images. To obtain the R_{rs} of the turbid water, we removed the atmospheric effects in the images using an iterative near-infrared atmospheric correction [29].

B. IDAS_{v2} Algorithm for IOPs Retrievals

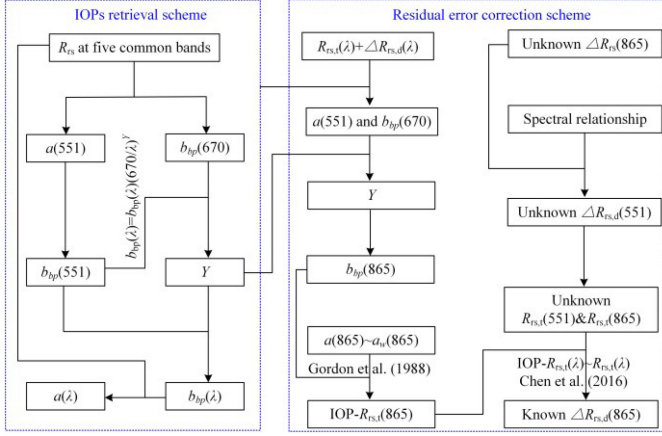
The IDAS_{v1} algorithm is a stepwise algorithm that first derives the absorption and backscattering coefficients at reference wavelengths from R_{rs} at four visible bands. Then the coefficient estimates are extended to the blue and red wavelengths after applying a spectral model of the particle backscattering coefficient (see detail in Appendix). However, the R_{rs} at visible bands is less sensitive to variation in the optically significant constituents than at the near-infrared bands for highly turbid water [24], so the stepwise process meaningfully combines $R_{rs}(865)$ into the IDAS_{v1} algorithm to retrieve IOPs from optically complex water. Furthermore, to accurately obtain b_b data from satellite R_{rs} data contaminated with the residual error, we do not estimate the power coefficient (Y) of the particle backscattering coefficient (b_{bp}) directly from R_{rs} at visible bands in the IDAS_{v1} scheme. Instead, we directly determine $b_b(670)$ from R_{rs} data. Directly determining $b_b(670)$ ensures that $b_b(670)$ might be highly accurate and be somewhat tolerant to the residual error in satellite R_{rs} , which is very important for estimating suspended sediment in turbid water [24], [33].

Based on those considerations for determining the two coefficients, we suggest the following conceptual models for estimating $a(551)$ and $b_b(670)$:

$$a(551) = f_{nn} [R_{rs}(443), R_{rs}(490), R_{rs}(551), \\ \times R_{rs}(670), R_{rs}(865)] \quad (1)$$

$$b_b(670) = g_{nn} [R_{rs}(443), R_{rs}(490), \\ \times R_{rs}(551), R_{rs}(670), R_{rs}(865)] \quad (2)$$

f_{nn} and g_{nn} are neural network models for the $a(551)$ and $b_b(670)$ estimates. When $a(551)$ is known, then $b_b(551)$ is determined from R_{rs} following the relationship between IOPs and R_{rs} as outlined by Gordon *et al.* [27]. Thus, Y is analytically

Fig. 2. Flowchart for the IDAS_{v2} algorithm.

determined as follows:

$$Y = 0.0849 \log \left[\frac{b_{bp}(551)}{b_{bp}(670)} \right]. \quad (3)$$

After applying the spectral model of the particle backscattering coefficient [34], $b_{bp}(670)$ can be extended to other wavelengths, which can be converted into the absorption coefficients by substituting into the IOPs– R_{rs} relationship (see Fig. 2).

The absorption of pure water at 865 nm is one order of magnitude larger than the absorption at 670 nm [34]. Moreover, the phytoplankton absorption can be ignored at near-infrared wavelengths compared with pure absorption [35], so the variations in $a(865)$ mainly depend on the sum of detritus and gelbstoff absorptions (a_{dg}). Generally, the $a_{dg}(865)$ is far smaller than $a_{dg}(670)$ due to the exponential decrease of particle absorption as wavelengths decrease [5]. Carder *et al.* [36], Kowalczyk *et al.* [37], Tiwari and Shanmugam [38], and Hancke *et al.* [39] showed that, from historical precedence, the average of the spectral slope for a_{dg} is between 0.014 and 0.015 nm⁻¹, so $a_{dg}(670)$ is more than one order of magnitude larger than $a_{dg}(865)$. Thus, the ratio of a_{nw} to a at 865 nm is at least two orders of magnitude smaller than the ratio to a at 670 nm. In other words, to correct for residual errors for turbid water, it is more advantageous to use the 865 nm band than the 670 nm band because it is easier to accurately obtain $R_{rs}(865)$ than $R_{rs}(670)$ using the IOPs– R_{rs} relationship [29]. Thus, we suggest using the 865 nm band instead of the 670 nm band in IDAS_{v2} to correct for the residual errors for turbid water (see Fig. 2).

C. Statistical Criteria

In this study, we used the mean absolute percent difference (MAPD), root-mean-square of the log transformed error (RMSE_{log}), and unbiased mean relative error to assess the accuracy of the IOPs retrieval algorithms. These statistics are expressed as follows:

$$\text{MAPD} = \frac{1}{n} \sum_{i=1}^n \left| \frac{x_{nc,i} - x_{c,i}}{x_{c,i}} \right| \times 100\% \quad (4)$$

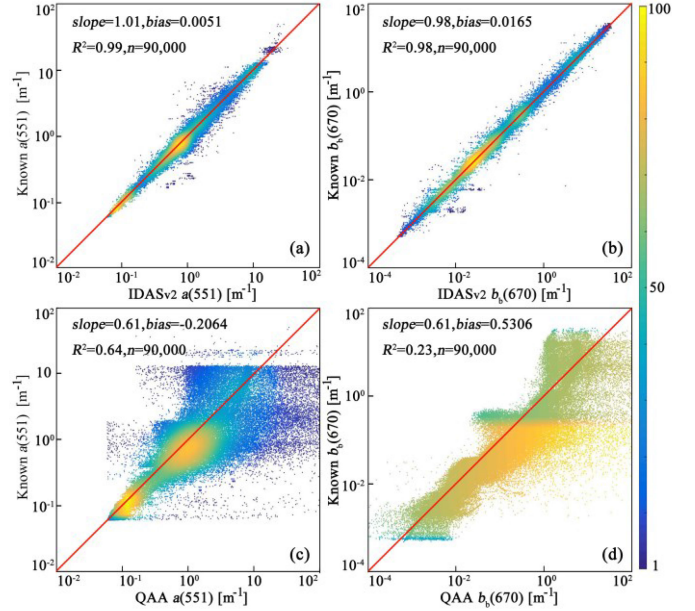


Fig. 3. Scatterplots of model-derived versus known $a(551)$ and $b_b(670)$ for the synthetic dataset. (a) and (b) Results obtained with the IDAS_{v2} algorithm. (c) and (d) Results obtained with the QAA algorithm. The “known” values are from the Hydrolight simulations.

$$\text{UMRE} = \frac{1}{n} \sum_{i=1}^n \left| \frac{x_{nc,i} - x_{c,i}}{0.5x_{nc,i} + 0.5x_{c,i}} \right| \times 100\% \quad (5)$$

$$\text{RMSE}_{\log} = \frac{1}{n} \sqrt{\sum_{i=1}^n [\log(x_{nc,i}) - \log(x_{c,i})]^2} \quad (6)$$

$x_{nc,i}$ is the IOPs product of the i th element provided by retrieval model. $x_{c,i}$ is the equivalent product of the i th element provided by Hydrolight and *in situ* measurements. x_m is the mean of the absorption coefficients for a 3×3 box, and n is the number of elements.

III. RESULTS AND DISCUSSION

A. Training the IDAS_{v2} Algorithm With the Synthetic Dataset

Two neural network models in the IDAS_{v2} algorithm retrieve $a(551)$ and $b_b(670)$ from R_{rs} at five “common bands” in the second-generation ocean color satellites. For the purpose of prediction, we trained two models using the synthetic dataset that included errors in R_{rs} (see Table I). The scatterplots in Fig. 3(a) and (b) present the $a(551)$ and $b_b(670)$ that we derived from the synthetic dataset versus the known Hydrolight $a(551)$ and $b_b(670)$, respectively. We found that, even though large random residual errors were added into R_{rs} (e.g., $\sim 37\%$ random uncertainty at 670 nm band), the neural network models estimated $a(551)$ and $b_b(670)$ well, at least for this specific synthetic dataset. Most points of the model-derived data and known values centered around the 1:1 line, and the coefficients of determination (R^2) were no lower than 0.98. These results indicate that the two neural network models effectively derived $a(551)$ and $b_b(670)$ from our error-included R_{rs} .

Fig. 3(c) and (d) shows the scatterplots of the QAA model-derived versus the known $a(551)$ and $b_b(670)$ for the same synthetic dataset that contained the errors. Overall, the QAA algorithm performed well for the moderately turbid water, but it is hard for us to explain the variation in the IOPs for the extremely turbid waters. The difficulty arose because of the following.

- 1) The QAA algorithm was originally designed to retrieve IOPs from the open ocean [18] and from moderately turbid water [40], and it might not have been technically correct to apply the QAA algorithm to the optically complex turbid water.
- 2) The R_{rs} at visible bands became less sensitive to the variations of optically significant constituents in the highly turbid water [24].
- 3) There are many band ratio approaches in the QAA algorithm, which made the algorithm very sensitive to the residual errors in the R_{rs} data for clear or turbid water [20].

After comparing the IDAS_{v2} algorithm results to the QAA algorithm results, we found that IDAS_{v2} more effectively retrieved IOPs. Specifically, at the higher end ($a(551) > 2 \text{ m}^{-1}$), there was no statistically significant relationship between QAA-derived and known $a(551)$, but the IDAS_{v2} algorithm significantly strengthened the relationship between its derived $a(551)$ and the known $a(551)$.

We noted that the QAA algorithm more effectively retrieved $a(551)$ than it did $b_b(670)$ [see Fig. 3(c) and (d)]. For example, the statistical relationship between the QAA-derived and the known $a(551)$ is much more significant than the same relationship for the algorithm-derived and known $b_b(670)$ values. This discrepancy between the a and b relationships exists because of the IOPs- R_{rs} relationship in the QAA algorithm, which causes the uncertainty in $a(551)$ and the R_{rs} data to propagate to $b_b(670)$.

B. Algorithm Evaluation and Comparison

1) *Testing the Algorithms for Open Ocean Water:* We evaluated the performance of the IOPs retrieval algorithms by comparing the predicted IOPs produced by the algorithms to equivalent field measurements. Table I describes that water bodies from the oceanic dataset had wide dynamic ranges of optical properties. For example, $a(551)$ varied from 0.0597 to 26.0632 m^{-1} , and $b_b(670)$ varied from 0.0004 to 5.2761 m^{-1} . Fig. 4 shows how well the IDAS_{v2} and QAA algorithms estimated $a(551)$ and $b_b(670)$ from global oceanic waters when we ran the algorithms with the oceanic dataset. The results indicate that the IDAS_{v2} algorithm effectively derived IOPs from the clear open ocean and from turbid coastal water. Specifically, the IOPs derived from the algorithm agreed very well with their equivalent *in situ* measurements, and the determination coefficients were all greater than 0.55. After comparing the IDAS_{v2} model results to the QAA model results, we found that IDAS_{v2} more effectively retrieved $a(551)$ and $b_b(670)$. The MAPD values of the $a(551)$ and $b_b(670)$ that we retrieved with the IDAS_{v2} algorithm were less than 28.36% and were much lower than the MAPDs of the $a(551)$ and $b_b(670)$ that the QAA algorithm produced.

For most oceanic waters, including the open ocean and some moderately turbid coastal water, the QAA algorithm can

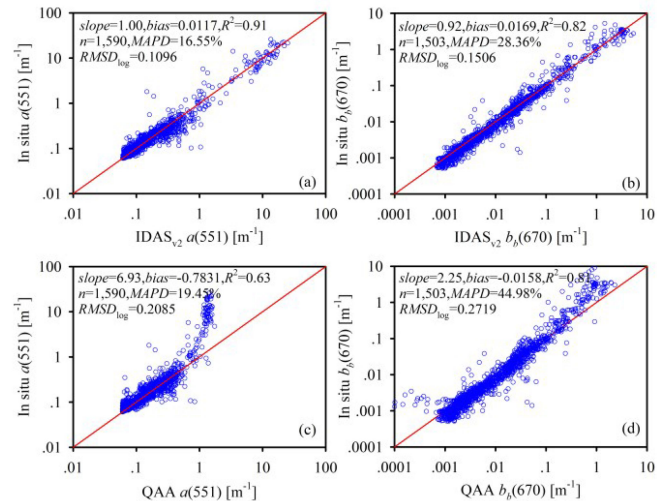


Fig. 4. Comparison of field-measured with model-derived $a(551)$ and $b_b(670)$ for the oceanic dataset. (a) and (b) Results from the IDAS_{v2} algorithm. (c) and (d) Results from the QAA algorithm.

determine ($a(551) < 0.5 \text{ m}^{-1}$), $a(551)$ with high accuracy ($\sim 16\%$ MAPD value). Usually, the field measurements for R_{rs} contain substantial uncertainty even though rigorous protocols were followed for experiment deployment and data collection (Mueller *et al.* 2003). Because $b_b(670)$ and $R_{rs}(670)$ are very small for the open ocean [20], a small absolute uncertainty in the $R_{rs}(670)$ data can lead to very large errors in retrieving $b_b(670)$ when using the QAA algorithm. Consequently, many scatterplots of field-measured versus QAA algorithm-derived $b_b(670)$ deviated significantly from the 1:1 line at the lower end ($< 0.002 \text{ m}^{-1}$), even though the QAA algorithm performed well at retrieving $a(551)$ from oceanic waters. These results confirm that the QAA algorithm is not noise tolerant for IOP retrievals, at least for $b_b(670)$ in the open ocean.

The QAA algorithm was originally developed to retrieve IOPs from clear and moderately turbid waters [5], even though there already were successful cases of retrieving IOPs from some natural turbid water [41]–[43]. However, the optical properties of natural turbid water are quite different from the optical properties of clear and moderately turbid water [16], [24], [44]. This means that the QAA algorithm might produce unexpected results when retrieving $a(551)$ and $b_b(670)$ from turbid water. Fig. 4(c) shows that the QAA algorithm was less effective at retrieving IOPs from turbid water than from the open ocean. Specifically, the QAA algorithm significantly underestimated $a(551)$ when $a(551)$ was more than 0.9 m^{-1} . When we excluded the data samples with $a(551) > 0.9 \text{ m}^{-1}$, the MAPDs for the QAA algorithm results decreased to 16.28%, and were comparable to the MAPDs of the IDAS_{v2} algorithm estimates for $a(551)$.

Fig. 4(d) shows that $b_b(670)$ was underestimated at the higher end ($b_b(670) > 0.1 \text{ m}^{-1}$). Underestimating $a(551)$ can lead to underestimating $b_b(551)$ from $R_{rs}(551)$ when using the QAA algorithm according to the IOPs- R_{rs} relationship [27] when $R_{rs}(551)$ remains constant. Because the ratio of the 670–551 nm wavelengths was very close to 1.0 (~ 0.83), a large uncertainty in the computing Y retrievals gives only a very small error when extrapolating $b_b(670)$ from $b_b(551)$ using the power model

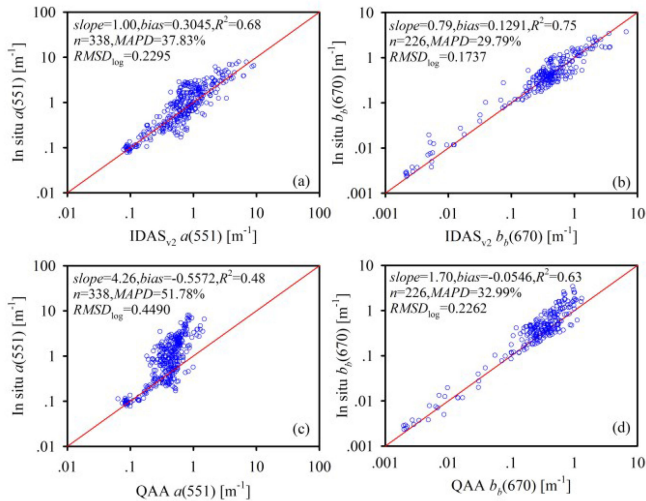


Fig. 5. Comparing field-measured with model-derived $a(551)$ and $b_b(670)$ for the inland lake dataset. (a) (b) Results from the IDAS_{v2} algorithm. (c) and (d) Results from the QAA algorithm.

[34], [40]. Thus, the underestimation of $a(551)$ can lead to underestimation of $b_b(670)$ in QAA results. By comparison, the IDAS_{v2} algorithm interpreted the variations of $a(551)$ and $b_b(670)$ from the open ocean and turbid coastal water by significantly improving the systematic bias in the QAA results at the higher end [see Fig. 4(a) and (b)]. Thus, we concluded that the IDAS_{v2} algorithm effectively derives $a(551)$ and $b_b(670)$ from water with a wide range of optical properties.

2) *Testing the Algorithms for Lakes:* Generally, the chlorophyll-a concentration in lakes has a much wider dynamic range than in the open ocean and coastal waters [45]. Table I describes that $b_b(670)$ in our oceanic dataset varied from 0.0004 to 5.2761 m^{-1} , which was a $\sim 50\%$ wider range than our lake dataset, but the dynamic range of the power coefficient was 20% narrower than the lake's. These results indicate that the optical properties of inland lakes are quite different from the optical properties of oceanic waters. Thus, it might be interesting to show how robust the IDAS_{v2} algorithm is when retrieving IOPs retrievals for these inland waters.

Fig. 5 compares the $a(551)$ and $b_b(670)$ derived with the IDAS_{v2} algorithm to the measured $a(551)$ and $b_b(670)$ from the inland lake dataset. We found that the IDAS_{v2} algorithm derived the two coefficients very well from inland lakes data without our having to reconfigure the neural network models in the algorithm. Specifically, the MAPDs for the $a(551)$ and $b_b(670)$ retrievals were 37.84% and 29.79%, respectively. The R^2 values were no lower than 0.68 [see Fig. 5(a) and (b)], which means that the IDAS_{v2} algorithm interpreted at least 68% of the variations in $a(551)$ and $b_b(670)$ for the inland waters. According to the average $a(551)$ and $b_b(670)$ listed in Table I, overall, our inland lake data were much more turbid than the oceanic water. This could be why the MAPDs of the IDAS_{v2} algorithm for the oceanic waters were clearly lower than for the lakes (see Figs. 4 and 5).

Like its performance for the oceanic and coastal waters, the QAA algorithm was robust at retrieving $a(551)$ from moderately

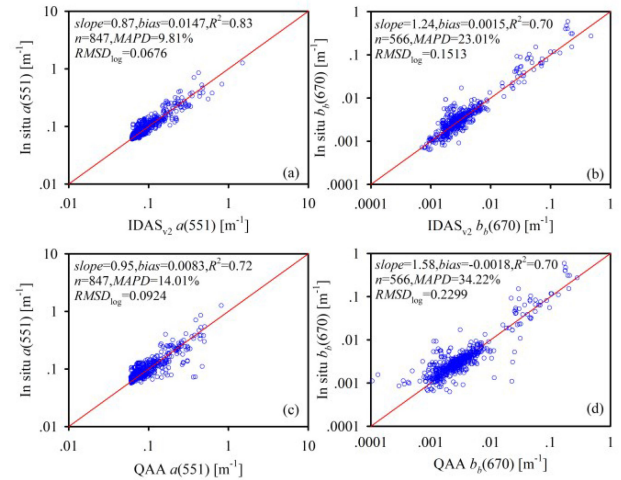


Fig. 6. Comparing field-measured with satellite-observed $a(551)$ and $b_b(670)$ for the matchup dataset. (a) and (b) Results from the IDAS_{v2} algorithm. (c) and (d) Results from the QAA algorithm.

turbid waters ($a(551) < 0.2 \text{ m}^{-1}$), but the algorithm seriously underestimated $a(551)$ for the turbid water ($a(551) > 0.3 \text{ m}^{-1}$). The critical point where $a(551)$ transitioned from an underestimate to an overestimate for oceanic waters was ~ 3 times larger than for the inland waters, indicating that the optical properties of the lake dataset might have been more complicated than the optical properties of the oceanic dataset. With the constraint of the IOPs– R_{rs} relationship, underestimating $a(551)$ can result in $b_b(670)$ being underestimated [see Fig. 5(c)], which is consistent with the results in Fig. 4(c) and (d). Consequently, the $b_b(670)$ that the model derived was significantly lower at its higher end ($> 0.1 \text{ m}^{-1}$) than the $b_b(670)$ measured in the field [see Fig. 5(d)]. By comparison, the QAA and IDAS_{v2} algorithms were applicable to the IOPs retrievals from the inland lakes, but the IDAS_{v2} algorithm was more effective than the QAA algorithm, for our dataset. The IDAS_{v2} algorithm derived $a(551)$ and $b_b(670)$ whose MAPDs were 13.95% and 3.20% lower, respectively, than the MAPDs for the IOPs derived by the QAA algorithm.

C. Matchup Dataset Analysis and Comparison Between the IDAS_{v2} and QAA Algorithms

We implemented our matchup analysis by comparing field measurements to the IOPs derived from satellite data using our two algorithms. Fig. 6 shows the satellite-derived data plotted against the IOPs measured in the field, indicating that the IDAS_{v2} and QAA algorithms generated IOPs that were consistent with the field measurements. Specifically, the MAPDs did not exceed 34.22%, and the corresponding R^2 was no lower than 0.70 meaning that the IDAS_{v2} or QAA algorithms interpreted $> 70\%$ of the variance in the IOPs from the satellite R_{rs} data. However, the IDAS_{v2} algorithm more effectively derived IOPs from the satellite R_r than the QAA algorithm did. The MAPD values for $a(551)$ and $b_b(670)$ retrieved by the IDAS_{v2} algorithm were 4.2% and 11.21% less than the MAPDs for the QAA algorithm results, respectively. These results indicate that the IDAS_{v2}

algorithm can be used to retrieve IOPs from satellite R_{rs} for natural waters.

Because the IDAS_{v2} algorithm was designed to semianalytically derive IOPs from satellite R_{rs} , and, at the same time, to account for the residual errors in the satellite R_{rs} [20], [21], the IDAS_{v2} algorithm tolerates noise better than the QAA algorithm does. For example, many points in the scatterplots of the QAA results deviated from the 1:1 line, but the IDAS_{v2} algorithm results tended to gather around the 1:1 line. Furthermore, the QAA algorithm significantly underestimated $b_b(670)$ at the lower end ($<0.002 \text{ m}^{-1}$), which is consistent with the results presented in Fig. 4.

We noted that the dynamic ranges of the IOPs in the matchup dataset were narrower than in the oceanic and lake datasets (see Table I). This is because most of the data in the matchup dataset were collected from clear and moderately turbid waters. As a result, the MAPDs for the IDAS_{v2} algorithm results from the matchup datasets were significantly smaller than from the oceanic and lake datasets (see Figs. 4–6). Those matchup data results indicate that optical complexity can influence the performance of the IDAS_{v2} algorithm, but this influence was much less than the influence of optical complexity on the QAA algorithm.

D. Intermission Consistency Analysis

Due to imperfect data processing systems and sensor performance, satellite-observed R_{rs} always includes substantial residual errors and intermission biases [21], which can cause inconsistencies in the IOPs derived from different ocean color data. The IOPs derived from the data of one satellite-observed R_{rs} would be highly consistent with the IOPs derived from other satellite-observed R_{rs} data if the IDAS_{v2} algorithm could absorb the residual errors and intermission bias in the data. Therefore, we demonstrate how capable the IDAS_{v2} algorithm is at consistently producing $a(551)$ and $b_b(670)$ data from multiple missions.

Fig. 7 shows the IOPs derived from cloud free VIIRS and MERSI2 images on 17 April 2018. Both VIIRS and MERSI2 R_{rs} data were achieved using near-infrared and shortwave infrared bands combined atmospheric correction algorithm developed by Wang and Shi [46]. Chen *et al.* [32] showed that the MERSI2 instrument could provide accurate R_{rs} data comparable with the VIIRS in the turbid coastal waters. We found that $a(551)$ and $b_b(670)$ had large dynamic ranges in the Eastern China Coastal Seas. For example, the $a(551)$ varied from 0.0597 to 53.0889 m^{-1} with an average of 0.3588 m^{-1} , and $b_b(670)$ ranged from 0.0004 to 22.3044 m^{-1} with an average of 0.1090 m^{-1} . The highest $a(551)$ values exceeded 5 m^{-1} and were around the Oujian River Estuary, Hangzhou Bay, the Subei shoal patch, the Changjiang River Estuary, the Yellow River Estuary, and the Liaohe River Estuary. The lower $a(551)$ values of $<0.07 \text{ m}^{-1}$ were in the ocean far away from the coastline. The $b_b(670)$ data were spatially distributed like the $a(551)$ data whose values decreased from the coast to the open ocean [see Fig. 7(e) and (f)]. This spatial decreasing pattern was due to strong tidal currents and other factors discharging sediment from the land into the outer estuary [47].

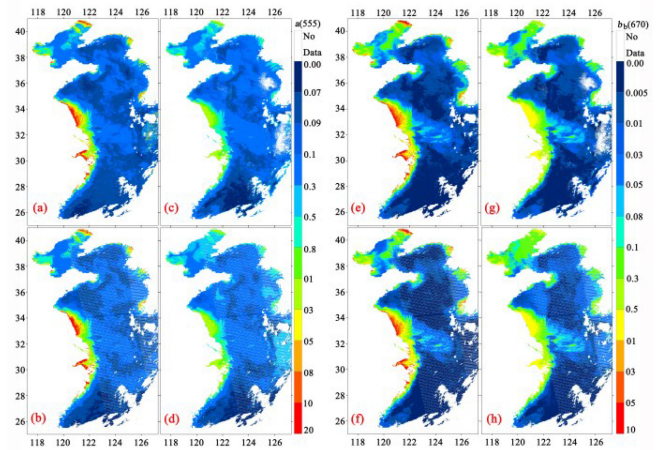


Fig. 7. Different satellite observed (a)–(d) $a(551)$ and (e)–(h) $b_b(670)$ from R_{rs} data. The top four images were MERSI2 results, while the bottom four images were VIIRS results. (a) and (b), and (c) and (d) IDAS_{v2} and QAA $a(551)$, respectively; while (e) and (f), and (g) and (h) IDAS_{v2} and QAA $b_b(670)$, respectively. The white colored patches are clouds or land.

Overall, the $a(551)$ and $b_b(670)$ derived with the QAA algorithm were patterned spatially like the IDAS_{v2} IOPs results for the Eastern China Coastal Seas. For example, the IOPs of the coastal regions were much higher than those of the open ocean [see Fig. 7(c) and (d), and (g) and (h)]. However, because the QAA algorithm routinely underestimates values at the higher end (see Figs. 4 and 5), the QAA IOPs were much lower than the retrieved IDAS_{v2} IOPs. Specifically, the $a(551)$ varied from 0.0597 to 4.0395 m^{-1} with an average of 0.2251 m^{-1} , and $b_b(670)$ ranged from 0.0001 to 1.7064 m^{-1} with an average of 0.0663 m^{-1} . Overall, the mean QAA $a(551)$ and $b_b(670)$ were $\sim 50\%$ lower than the mean IDAS_{v2} results, which indicates that the IDAS_{v2} algorithm can generate broad and flat IOP frequency distributions compared to results that the QAA algorithm provides.

Chen *et al.* [21] showed that the IDAS algorithm removed most of the residual error and partial intermission bias from IOPs estimates. Fig. 7 shows that the IDAS_{v2} algorithm provided consistent intermission IOPs from the VIIRS and MERSI2 instruments. For example, the estimates from the two instruments had similar spatial patterns with the same complex distribution of the IOPs such as tongue-shaped plumes in the same river estuary for each satellite image. Like in Fig. 7, Fig. 8(a) and (b) shows $a(551)$ and $b_b(670)$ that the IDAS_{v2} algorithm estimated in a box-by-box manner from the VIIRS and MERSI2 images. The box-by-box method effectively decreases pseudovariations in the satellite signals associated with mismatched geometry and instrumental random noise [32]. We found that, despite the satellite R_{rs} data being contaminated by residual errors and intermission bias, the IDAS_{v2} algorithm still performed well in providing consistent intermission IOPs data. Specifically, the points in the scatterplots of the VIIRS versus MERSI2 IOPs cluster around the 1:1 line, and the statistics show that the UMREs did not exceed 27.73%, even though the VIIRS $b_b(670)$ were systematically lower than the MERSI2 $b_b(670)$ at the lower end ($<0.01 \text{ m}^{-1}$).

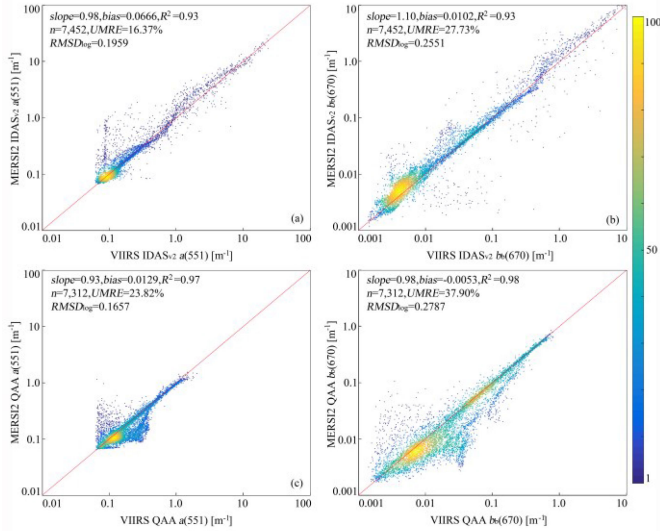


Fig. 8. As in Fig. 7, but for comparing intermission (a) and (b) IDAS_{v2} and (c) and (d) QAA IOPs in a box-by-box manner. (a) and (c) $a(551)$ while (b)–(d) $b_b(670)$ results.

Comparing VIIRS with MERSI2 QAA $a(551)$ and $b_b(670)$ [see Fig. 8(c) and (d)] indicates that the QAA algorithm provided consistent intermission IOPs data from optically complex water, even though many points deviated from the 1:1 line at the lower end [$<0.01 \text{ m}^{-1}$ for $b_b(670)$ and $<0.1 \text{ m}^{-1}$ for $a(551)$]. By comparison, the IDAS_{v2} algorithm provided more consistent intermission $a(551)$ or $b_b(670)$ results than the QAA algorithm, even for turbid coastal water. The intermission differences for $a(551)$ and $b_b(670)$ were 7.45% and 10.17% lower, respectively, when we used the IDAS_{v2} algorithm than the intermission difference when we used the QAA algorithm. Mélin [48] showed that it is hard to obtain the correct temporal change trend from multimission satellite data with $\pm 5\%$ intermission difference. Thus, improving the intermission consistency by $>7\%$ would be beneficial for learning about the impacts of global climate change on coastal ecology using continuous ocean color data from multimission satellites. In addition, using the QAA algorithm produced 140 ($\sim 1.9\%$ of the total valid samples) negative IOPs estimates (i.e., bad samples), which we excluded from the QAA results when we evaluated the statistics. If we had considered these “bad samples” in the uncertainty analysis, then the intermission difference of the QAA algorithm would have been significantly larger. Our results confirmed that the IDAS_{v2} and QAA algorithms effectively process ocean color data for retrieving IOPs, yet IDAS_{v2} performed significantly better than the QAA algorithm for our satellite data.

E. Compared IDAS_{v1} With IDAS_{v2} Algorithm in Residual Error Correction

Chen *et al.* [20] showed that the original IDAS (IDAS_{v1}) algorithm removes the residual error in satellite R_{rs} associated with imperfect atmospheric correction in the open ocean, as long as the spectral relationship of the residual error is known. However, we do not know if the IDAS_{v2} algorithm can correct for residual

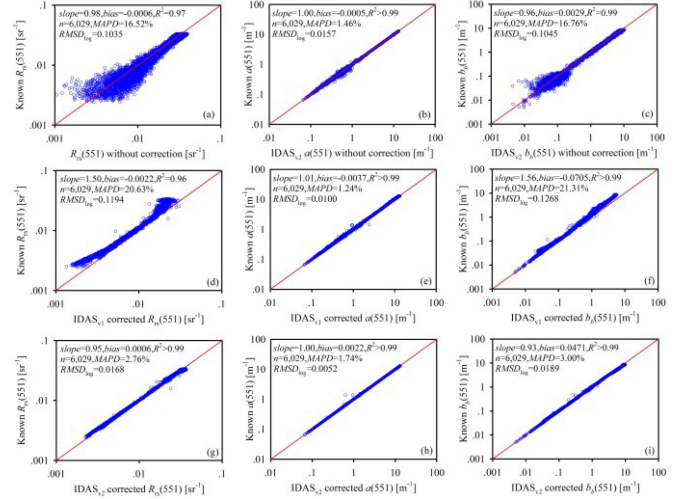


Fig. 9. Comparison of derived $a(551)$ and $b_b(551)$ from R_{rs} (a)–(c) before and (d)–(i) after residual error correction. (d)–(f) IDAS_{v1} results and (g)–(i) IDAS_{v2} results. “Known” represents $a(551)$ or $b_b(551)$ derived from error-free R_{rs} data.

errors in IOPs data from turbid waters. To account for this, we generated 6029 error-free R_{rs} spectra with Hydrolight, and we added random uncertainty into these R_{rs} data. Fig. 9(a) shows that there was 16.52% uncertainty in the $R_{rs}(551)$. Because the IDAS_{v2} algorithms was trained with R_{rs} data that included errors, the algorithm absorbed some of the effects of the residual errors in the R_{rs} and obtained good estimates of $a(551)$ from the turbid water [see Fig. 9(b)]. When we accurately determined the $a(551)$, the uncertainty in $R_{rs}(551)$ propagated to the $b_b(551)$ estimates following the relationship between IOPs and R_{rs} that Gordon *et al.* [27]. Thus, it is hard to accurately derive $b_b(551)$ from R_{rs} data before residual error correction [see Fig. 9(c)].

In the IDAS_{v1} algorithm, we corrected for the residual error for 670 nm, and we used a simple power approach to estimate $a_{nw}(670)$ from $a_{nw}(551)$ [20], [21], where a_{nw} was the total absorption minus absorption of pure water (a_w). In the open ocean, it is always acceptable to assume that $a_w \gg a_{nw}$ at 670 nm [34], so it is reasonable to ignore the impacts of $a_{nw}(670)$ retrieval uncertainty on $a(670)$ estimates. However, assuming $a_w \gg a_{nw}$ at 670 nm might not be true for highly turbid water because the absorption by particulate matter can be almost equal to or even much larger than $a_{nw}(670)$ in natural turbid water [49]. So the accuracy of the $a(670)$ estimate would significantly affect how well the IDAS_{v1} algorithm corrects for residual errors, but it is challenging to accurately determine $a(670)$ from turbid water due to the complex optical properties [34]. Consequently, after applying IDAS_{v1}, the data quality of R_{rs} and the IOPs products were even worse than the data quality when the data errors were not corrected [see Fig. 9(d) and (f)], and the systematic overestimates of $R_{rs}(551)$ and $b_b(551)$ are displayed in Fig. 9(d) and (f), respectively. As in Chen *et al.* [20], [21], we conclude that the IDAS_{v1} algorithm will work with residual errors in open ocean and some moderately turbid waters, but it might not work for a highly turbid environment unless we accurately know $a_{nw}(670)$.

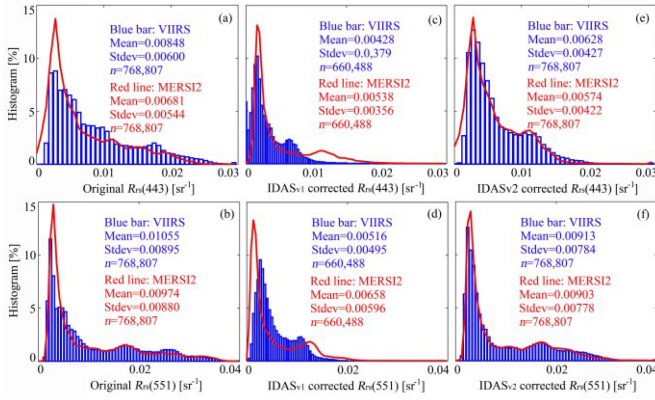


Fig. 10. Histograms of $R_{rs}(443)$ and $R_{rs}(551)$ values of the (a) and (b) original images. (c) and (d), and (e) and (f) images with residual error corrected using IDAS_{v1} and IDAS_{v2} algorithms, respectively.

Having the 865 nm band instead of the 670 nm band to correct for the residual error (see Fig. 2), Fig. 9(g) and (i) showed how well the IDAS_{v2} algorithm retrieved R_{rs} and the IOPs. We found that using IDAS_{v2} significantly improved the data quality of R_{rs} and the IOPs products. For example, for $a(551)$ varying from 0.0658 m^{-1} to 13.1346 m^{-1} , the MAPDs for $R_{rs}(551)$ and $b_b(551)$ were 2.76% and 3.00%, respectively. By comparison, the MAPDs for the IDAS_{v2} $R_{rs}(551)$ and $b_b(551)$ products were at least six times lower than the earlier version IDAS_{v1} algorithm. Specifically, the IDAS_{v1} $b_b(551)$ results at the higher end ($>1.0 \text{ m}^{-1}$) were clearly underestimated, but the IDAS_{v2} $b_b(551)$ data were consistent with known $b_b(551)$ for those data points. The underestimation occurred because assuming $a_w \gg a_{nw}$ at the 865 nm band was more acceptable than at the 670 nm band for highly turbid water. These results confirmed that the IDAS_{v2} algorithm can potentially improve R_{rs} and IOPs products for turbid waters.

We used VIIRS and MERSI2 images of the Eastern China Coastal Seas on 17 April 2018 to learn if the IDAS algorithm could remove the residual error uncertainty and partial intermission bias in satellite R_{rs} for turbid water. With the 443 and 551 nm bands, as examples, Fig. 10 compares the histogram of R_{rs} from the MERSI2 and VIIRS images before and after correcting for the residual error. For the original images, the intermission ratio of averaged VIIRS to MERSI2 R_{rs} were 1.25 and 1.08 at 443 and 551 nm, respectively, which means that the VIIRS $R_{rs}(443)$ and $R_{rs}(551)$ were 25% and 8% larger than the MERSI2 $R_{rs}(443)$ and $R_{rs}(551)$, respectively. The R_{rs} differences occurred for the two instruments even though the nominal ascending equator local crossing times for VIIRS and MERSI2 were very close. Similarly, due to nonnegligible $a_{nw}(670)$, it was hard to use IDAS_{v1} algorithm to remove the intermission difference in R_{rs} data in the turbid coastal waters, even though it worked well in the open oceans [21]. Specifically, a clear mismatch could be observed from Fig. 10(c) and (d) for $R_{rs}(443) > 0.009 \text{ sr}^{-1}$ or $R_{rs}(551) > 0.016 \text{ sr}^{-1}$, while the intermission ratios were 1.26 and 1.27 for $R_{rs}(443)$ and $R_{rs}(551)$, respectively. Fortunately, after applying the IDAS_{v2} algorithm, the intermission difference between the VIIRS and MERSI2 R_{rs} was minimized. For instance, IDAS_{v2}

produced a narrow and sharp frequency distribution of $R_{rs}(443)$ and $R_{rs}(551)$ compared to the distribution for the original data [see Fig. 10(e) and (f)]. After correcting for the residual error, the intermission ratios were 1.09 and 1.01 for $R_{rs}(443)$ and $R_{rs}(551)$, respectively, which were >0.15 and >0.07 times smaller than the original and IDAS_{v1} data. These results indicate that the IDAS_{v2} algorithm can potentially provide consistent intermission ocean color data from turbid water for climatic research due to its effectiveness in correcting for the residual error and partial intermission bias [21].

F. Discussion

Lee *et al.* (2009) used the red to blue band ratio approaches to derive absorption coefficients at reference bands in the QAA algorithm. In general data collection practice, remote sensing reflectance is derived from above-surface optical measurements, which include water-leaving radiance, sky radiance, and total incident radiance flux [30]. Because the total incident radiance flux can be accurately measured on cloud free days, the R_{rs} uncertainties originate from measuring uncertainties of the water-leaving radiance and from uncertainties from calculating the sky radiance in the water-leaving radiance [50]. Therefore, the uncertainties in R_{rs} measurements are more like additive uncertainties and have the spectrally dependent characteristics as described by the R_{rs} calculation equation [34]. In addition, Chen *et al.* [21] showed that the residual error in satellite R_{rs} is not a multiplying uncertainty, which is like the uncertainties in field measurements. Hu *et al.* [51] showed that the band difference approach is more advantageous than the band ratio approach for minimizing the spectrally related and additive uncertainties. Specifically, the practical field measurements indicate that field-measured R_{rs} always contains substantial uncertainties at red and near-infrared wavelengths. By merging the band difference approach into neural network models, the IDAS_{v2} algorithm can absorb the systematic spectrally dependent uncertainty in satellite or field R_{rs} and at least provide accurate $a(551)$ and $b_b(670)$ for natural waters (see Figs. 4 and 6).

Doxaran *et al.* [24], Volpe *et al.* [52], and Mao *et al.* [47] showed that the sensitivity of the red to blue band ratio decreases with increasing optically significant constituents for turbid water, so the near-infrared bands are usually suggested for IOPs retrieval from extremely turbid water [53]. Our study shows that IOPs can be accurately derived from turbid water using the IDAS_{v2} algorithm with near-infrared wavelengths. NASA's default data processing system determines R_{rs} for the open ocean using a near-infrared atmospheric correction method [2], and the data processing system determines R_{rs} for turbid water using an iterative near-infrared atmospheric correction approach [29]. The near-infrared approach assumes that the remote sensing reflectance at near-infrared wavelengths can be ignored due to the strong absorption by pure water in the open ocean, so there is always no near-infrared data for running the IDAS_{v2} algorithm. Therefore, combining IDAS_{v2} with IDAS_{v1} might be a good choice for retrieving IOPs from global natural waters; for example, deriving IOPs products from natural turbid waters (chlorophyll-a concentration $\geq 1.3 \mu\text{g l}^{-1}$) with the

IDAS_{v2} algorithm, and switching to the IDAS_{v1} algorithm for the open ocean (chlorophyll-a concentration $\leq 0.7 \mu\text{g l}^{-1}$). Note that the water-type classification results are consistent with the classification results used for iterative atmospheric correction [29], [54].

The IDAS_{v2} algorithm contains two components, the IOPs retrieval algorithm and the residual error correction algorithm. The retrieval algorithm provides highly accurate $a(551)$ and $b_b(670)$ data. When R_{rs} contains uncertainties, it is hard to accurately obtain $b_b(551)$ using the IOPs- R_{rs} relationship [18] so determining Y would contain some uncertainty using the relationship displayed in Fig. 2. The uncertainty in Y would lead to substantial uncertainty in the $b_b(\lambda)$ data, which is extrapolated from $b_b(670)$ using an exponential model [34]. From a trend analysis of $b_b(551)$, Chen *et al.* [21] showed that the residual errors and intermission bias can result in misleading conclusions. To obtain reliable $b_b(\lambda)$, the residual error in R_{rs} data must be removed (see Fig. 9), suggesting that, when processing the data, it is very important to correct for the residual error before retrieving the IOPs.

Table I describes that the $a(551)$ data vary from 0.0598 to 1.2657 m^{-1} , with a median of 0.0789 m^{-1} , indicating that the sample points in the matchup dataset varied from the clear to turbid waters, but most of these samples were from the open ocean (see Fig. 1). Thus, it is not surprising that the MAPDs for the matchup dataset were much lower than the MAPDs for the oceanic and lake datasets. The lower statistics occurred because the optical properties of clear water are much simpler than the optical properties of turbid water [55]. Consequently, it is very important to perform a matchup analysis with the IDAS_{v2} algorithm for highly turbid water. To achieve the needed signal to noise ratio for ocean color detection, the satellite's instrument is usually designed with a reasonable dynamic range for radiance collection. For extremely turbid water, the incoming radiance is so strong that the instrument's electrical signal is easily saturated or responds nonlinearly to the incoming radiance. Thus, it is hard to scientifically evaluate the accuracy of the ocean color products for extremely turbid water even though we employed a rigorous matchup analysis [31]. Fortunately, there are many optical instruments, such as Landsat-8 and Sentinel-2, with dynamic signal ranges that are much wider than ocean color instruments such as VIIRS and MERSI2. Moreover, Landsat-8 and Sentinel-2 have data around the same five "common bands" we defined in this study. Thus, with some adjustment, the IDAS_{v2} algorithm can be used to retrieve IOPs from Landsat-8 and Sentinel-2 images. We encourage researchers to evaluate how accurately IDAS_{v2} retrieves IOPs from Landsat-8 and Sentinel-2 data.

Due to the short lifespan of ocean color satellites, it is common to combine several successive missions into a single dataset to increase observation time scales beyond the limited lifetime of a single mission [56]. However, due to instrument noise and imperfect data processing procedures, it is hard to find two satellites with the same ocean color data. Chen *et al.* [21] suggested that the IDAS_{v1} algorithm could simultaneously remove the residual error in satellite R_{rs} to absorb the intermission bias and provide consistent intermission ocean color products for

the open ocean. However, the open ocean occupies $\sim 78\%$ of the global ocean area [51]. Even though coastal waters only account for $\sim 32\%$ of global ocean area, global coastal waters support 90% of the world's fish catches [57] and are important ecosystems impacted by global climate change [58]. Ocean color data, including R_{rs} and IOPs, are essential variables of the global climate observation system [59]. Consistent intermission ocean color data are required to understand the long-term impacts of the climate change on the ecology of natural turbid waters. Fig. 10 indicates that the IDAS_{v2} algorithm can provide the consistent intermission ocean color data for turbid coastal waters. Our confidence in the results that we acquired from applying multimission ocean color data at climatic time scales lies in the algorithm's accuracy and intermission consistency [21]. The results of our analysis confirmed that the IDAS_{v2} algorithm can improve the robustness of the long-term multimission ocean color data. It is noteworthy that the different satellite platforms might have some difference in nearinfrared bands, so the band shifting for R_{rs} at near-infrared bands should be corrected before running the IDAS_{v2} algorithm for residual error correction.

IV. CONCLUSION

Accurate and consistent intermission IOPs data are critical to understanding the impacts of global climate change on the ecology of natural turbid waters. We proposed using the near-infrared bands to improve the performance of the IDAS_{v1} algorithm for retrieving IOPs from and correcting residual error in satellite images of natural turbid waters. We called the updated (Version 2) algorithm, IDAS_{v2}. In the IDAS_{v2} algorithm, two neural network models first determine $a(551)$ and $b_b(670)$ and then the estimates are used to calculate $b_b(551)$ and construct a power model for the particle backscattering coefficient. The IOPs at other wavelengths are obtained from the R_{rs} data after adopting the power model for the particle backscattering coefficient. Finally, the derived IOPs data are used to remove any residual error in the satellite R_{rs} data of the natural turbid water. It is important to note that we used the 865 nm band instead of the 670 nm band to correct for the residual error because it is much easier to accurately determine $a(865)$ than $a(670)$ from those waters. Determining $a(865)$ is easier because the pure water absorption coefficient at 865 nm is about one order of magnitude larger than the pure water absorption coefficient at 670 nm.

We evaluated the stability and accuracy of the new IDAS_{v2} algorithm using synthetic data, field measurements, and satellite images, all covering a wide and varied range of optical properties. We found that applying the IDAS_{v2} algorithm to field measurements and the satellite data resulted in our more effectively retrieving IOPs and correcting the residual error correction than when we used the QAA algorithm for natural waters. For example, when we tested our algorithm with bio-optical datasets collected from global oceanic waters and inland lakes, the R^2 values between the IOPs derived with the IDAS_{v2} algorithm and known IOPs were no lower than 0.68, and the corresponding MAPDs did not exceed 38%. Furthermore, after applying the IDAS_{v2} algorithm to correct for the residual error from VIIRS

and MERSI2 images, the residual error and partial intermission bias in the satellite R_{rs} data were effectively removed, and the VIIRS IOPs were consistent with the MERSI2 IOPs. All these results confirm that the IDAS_{v2} algorithm potentially provides accurate and consistent intermission IOPs for natural turbid water. Although we still need to validate the corrected data products, these preliminary results are encouraging and indicate that the IDAS_{v2} algorithm can provide high-quality IOPs data with intermission consistency.

APPENDIX A

BRIEF DESCRIPTION OF IDAS_{v1} ALGORITHM

With properly parameterized, Chen *et al.* [20], [49] suggested the following conceptual models for estimating $a(551)$ and $b_b(670)$:

$$a(551) = P_{nn} [R_{rs}(443), R_{rs}(490), R_{rs}(551), R_{rs}(670)] \quad (A1)$$

$$Y = Q_{nn} [R_{rs}(443), R_{rs}(490), R_{rs}(551), R_{rs}(670)] \quad (A2)$$

where P_{nn} and Q_{nn} are neural network models for the $a(551)$ and $b_b(670)$ estimates. Considering the residual errors in satellite R_{rs} (ΔR_{rs}), the IOPs- R_{rs} relationship can be revised as [20], [21] follows:

$$g_0 \frac{b_b(\lambda_1)}{a(\lambda_1) + b_b(\lambda_1)} + g_1 \left[\frac{b_b(\lambda_1)}{a(\lambda_1) + b_b(\lambda_1)} \right]^2 = \frac{R_{rs}(\lambda_1) - m_0 \Delta R_{rs}(\lambda_2) - m_1}{0.52 + 1.7 [R_{rs}(\lambda_1) - m_0 \Delta R_{rs}(\lambda_2) - m_1]} \quad (A3)$$

$$g_0 \frac{b_b(\lambda_2)}{a_w(\lambda_2) + b_b(\lambda_2)} + g_1 \left[\frac{b_b(\lambda_2)}{a_w(\lambda_2) + b_b(\lambda_2)} \right]^2 = \frac{R_{rs}(\lambda_2) - \Delta R_{rs}(\lambda_2)}{0.52 + 1.7 [R_{rs}(\lambda_2) - \Delta R_{rs}(\lambda_2)]} \quad (A4)$$

where g_0 and g_1 are known empirical coefficients [27], while m_0 and m_1 are known spectral relationship of residual errors. λ_1 and λ_2 are two wavelengths, which are 551 and 670 nm for IDAS_{v1} algorithm, but are 551 and 865 nm for IDAS_{v2} algorithm. When $a(\lambda_1)$ and Y are known, (A3) and (A4) would only contain two unknowns [$b_b(\lambda_1)$ and $\Delta R_{rs}(\lambda_2)$], which can be solved algebraically for each satellite R_{rs} spectrum [20], [21].

ACKNOWLEDGMENT

The authors would like to thank NASA for providing the ocean color data. They would also like to thank Dr. C. Huang from Nanjing Normal University, Dr. Y. Chen from National Marine Environmental Monitoring Center, and Dr. Z. Yu from Hangzhou Normal University for providing IOPs data from the Hangzhou Bay and Taihu Lake.

REFERENCES

- [1] H. R. Gordon, D. K. Clark, J. L. Mueller, and W. A. Hovis, "Phytoplankton pigments derived from the Nimbus-7 CZCS: Initial comparisons with surface measurements," *Science*, vol. 210, pp. 63–66, 1980.
- [2] H. R. Gordon and K. J. Voss, "Normalized water-leaving radiance, MODIS Algorithm Theoretical Basis Document (ATBD-17), 1999.
- [3] K. L. Carder, F. R. Chen, J. P. Cannizzaro, J. W. Campbell, and B. G. Mitchell, "Performance of the MODIS semi-analytical ocean color algorithm for chlorophyll-a," *Adv. Space Res.*, vol. 33 pp. 1152–1159, 2004.
- [4] I. S. Robinson, *Measuring the Oceans from Space: The principles and Methods of Satellite Oceanography*, Norfolk, VA, USA: Springer, 2003.
- [5] IOCCG, "Remote sensing of inherent optical properties: Fundamentals, tests of algorithms, and applications," Reports Number: ISSN 1098-6030, Reports of the International Ocean Colour Coordinating Group. No. 5, IOCCG, Dartmouth, NS, Canada., 2006.
- [6] S. W. Effler, F. Peng, D. M. O'Donnell, and C. Strait, "The backscattering coefficient and its components in the great lakes: A review and synthesis," *J. Great Lakes Res.*, vol. 39, pp. 108–122, 2013.
- [7] G. Zheng and P. M. DiGiacomo, "Remote sensing of chlorophyll-a in coastal waters based on the light absorption coefficient of phytoplankton," *Remote Sens. Environ.*, vol. 201, pp. 331–341, 2017.
- [8] D. Mckee and A. Cunningham, "Identification and characterisation of two optical water types in the Irish sea from in situ inherent optical properties and seawater constituents," *Estuarine Coastal Shelf Sci.*, vol. 68, pp. 305–316, 2006.
- [9] E. A. Loos and M. Costa, "Inherent optical properties and optical mass classification of the waters of the strait of Georgia, British Columbia, Canada," *Prog. Oceanogr.*, vol. 87, pp. 144–156, 2010.
- [10] R. Rottgers, C. Dupouy, B. B. Taylor, A. Bracher, and S. B. Wozniak, "Mass-specific light absorption coefficients of natural aquatic particles in the near-infrared spectral region," *Limnol. Oceanogr.*, vol. 59, pp. 1449–1460, 2014.
- [11] X. Xing, A. Morel, H. Claustre, F. D'Ortenzio, and A. Poteau, "Combined processing and mutual interpretation of radiometry and fluorometry from autonomous profiling bio-argo floats: 2. Colored dissolved organic matter absorption retrieval," *J. Geophysical Res.-Oceans*, vol. 117, 2012, pp. 2310–2317, Art. no. C04022.
- [12] A. Cunningham, L. Ramage, and D. McKee, "Relationships between inherent optical properties and the depth of penetration of solar radiation in optically complex coastal waters," *J. Geophys. Res.*, vol. 118, 2013.
- [13] Y. Zhang, Y. Yin, M. Wang, and X. Liu, "Effect of phytoplankton community composition and cell size on absorption properties in eutrophic shallow lakes: Field and experimental evidence," *Opt. Express*, vol. 20, pp. 11882–11898, 2012.
- [14] J. W. B. Robert *et al.*, "The influence of temperature and community structure on light absorption by phytoplankton in the North Atlantic," *Sensors*, vol. 19, 2019, Art. no. 4182.
- [15] W. P. Bissett, K. L. Carder, J. J. Walsh, and D. A. Dieterle, "Carbon cycling in the upper waters of the Sargasso sea: II. Numerical simulation of apparent and inherent optical properties," *Deep Sea Res. Part I: Oceanographic Res. Papers*, vol. 46, pp. 271–317, 1999.
- [16] P. J. Werdell *et al.*, "An overview of approaches and challenges for retrieving marine inherent optical properties from ocean color remote sensing," *Prog. Oceanogr.*, vol. 160, pp. 186–212, 2018.
- [17] S. A. Garver and D. Siegel, "Inherent optical property inversion of ocean color spectra and its biogeochemical interpretation I. Time series from the Sargasso sea," *J. Geophys. Res.*, vol. 102, pp. 18607–18625, 1997.
- [18] Z. P. Lee, K. L. Carder, and R. A. Arnone, "Deriving inherent optical properties from water color: A multi-band quasi-analytical algorithm for optically deep waters," *Appl. Opt.*, vol. 41, no. 27, pp. 5755–5772, 2002.
- [19] T. J. Smyth, G. F. Moore, T. Hirata, and J. Aiken, "Semi-analytical model for the derivation of ocean color inherent optical properties: Description, implementation, and performance assessment," *Appl. Opt.*, vol. 45, no. 31, pp. 8116–8132, 2006.
- [20] J. Chen, Z. P. Lee, C. M. Hu, and J. W. Wei, "Improving satellite data products for open oceans with a scheme to correct the residual errors in remote sensing reflectance," *J. Geophysical Res.-Ocean*, vol. 121, pp. 3866–3886, 2016.
- [21] J. Chen, X. Q. He, X. G. Xing, Q. G. Xing, Z. L. Liu, and D. L. Pan, "An inherent optical properties data processing system for achieving consistent ocean color products from different ocean color satellites," *J. Geophysical Res.-Ocean*, vol. 125, pp. 1–30, 2019.
- [22] J. Aiken, G. F. Moore, C. C. Trees, S. B. Hook, and D. K. Clark, "The SeaWiFS CZCS-type pigment algorithm," Goddard Space Flight Center, Greenbelt, MD, USA, SeaWiFS Tech. Rep. Ser. 104566, vol. 29, 1995.
- [23] X. Q. He, D. L. Pan, and Z. H. Mao, "Atmospheric correction of SeaWiFS imagery for turbid coastal and inland waters," *Acta Oceanologica Sinica*, vol. 33, pp. 609–615, 2004.

- [24] D. Doxaran, J. M. Froidefond, S. Lavender, and P. Castaing, "Spectral signature of highly turbid water application with SPOT data to quantify suspended particulate matter concentration," *Remote Sens. Environ.*, vol. 81, no. 1, pp. 149–161, 2002.
- [25] B. Han *et al.*, "Development of a semi-analytical algorithm for the retrieval of suspended particulate matter from remote sensing over clear to very turbid waters," *Remote Sens.*, vol. 8, pp. 1–23, 2016.
- [26] H. Z. Liu, Q. M. Zhou, Q. Q. Li, S. B. Hu, T. Z. Shi, and G. F. Wu, "Determining switching threshold for NIR-SWIR combined atmospheric correction algorithm of ocean color remote sensing," *ISPRS J. Photogrammetry Remote Sens.*, vol. 153, pp. 59–73, 2019.
- [27] H. R. Gordon, O. B. Brown, R. H. Evans, J. W. Brown, R. C. Smith, and K. S. Baker, "A semi-analytic radiance model of ocean color," *J. Geophysical Res.*, vol. 93, pp. 10909–10924, 1988.
- [28] C. D. Mobley and L. K. Sundman, *HydroLight 5.2 User's Guide*. Bellevue, WA, USA: Sequoia Scientific, 2013.
- [29] S. W. Bailey, F. A. Bryan, and P. J. Werdell, "Estimation of near-infrared water-leaving reflectance for satellite ocean color data processing," *Opt. Express*, vol. 18, pp. 7521–7527, 2010.
- [30] J. L. Mueller, G. S. Fargion, and C. R. McClain, *Ocean Optics Protocols For Satellite Ocean Color Sensor Validation*, Revision 4, NASA, Goddard Space Flight Center, Greenbelt, MD, USA, 2003.
- [31] S. W. Bailey and P. J. Werdell, "A multi-sensor approach for the on-orbit validation of ocean color satellite data products," *Remote Sens. Environ.*, vol. 102, pp. 12–23, 2006.
- [32] J. Chen *et al.*, "An approach to cross-calibrating multi-mission satellite data for open ocean," *Remote Sens. Environ.*, vol. 246, 2020, Art. no. 111895.
- [33] W. Shi and M. Wang, "Ocean reflectance spectra at the red, near-infrared, and shortwave infrared from highly turbid waters: A study in the Bohai sea, Yellow sea, and East China sea," *Limnol. Oceanogr.*, vol. 59, pp. 427–444, 2014.
- [34] C. D. Mobley, *Light and Water: Radiative Transfer in Natural Waters*. New York, NY, USA: Academic, 1994.
- [35] A. A. Gitelson *et al.*, "A simple semi-analytical model for remote estimation chlorophyll-a turbid waters: Validation," *Remote Sens. Environ.*, vol. 112, pp. 3582–3593, 2008.
- [36] K. L. Carder, F. R. Chen, Z. P. Lee, and S. K. Hawes, "Semi-analytical moderate resolution imaging spectrometer algorithms for chlorophyll a and absorption with bio-optical domains based on nitrate-depletion temperatures," *J. Geophysical Res.*, vol. 104, pp. 5403–5421, 1999.
- [37] P. Kowalczuk, C. A. Stedmon, and S. Markager, "Modeling absorption by CDOM in the Baltic sea from season salinity and chlorophyll," *Marine Chem.*, vol. 101, pp. 1–11, 2006.
- [38] S. P. Tiwari and P. Shanmugam, "An optical model for the remote sensing of coloured dissolved organic matter in coastal/ocean waters," *Estuarine, Coastal Shelf Sci.*, vol. 93, pp. 396–402, 2011.
- [39] K. Hancke *et al.*, "Optical properties of CDOM across the polar front in the barents sea: Origin, distribution and significance," *J. Marine Syst.*, vol. 130, pp. 219–227, 2014.
- [40] Z. P. Lee, P. J. Werdell, and R. Arnone, "An Update of the Quasi-Analytical Algorithm (QAA_V5), IOCCG Software Report. 2009. [Online]. Available: www.ioccg.org/groups/software_OCA.
- [41] S. Li, K. Song, G. Mu, Y. Zhao, J. Ma, and J. Ren, "Evaluation of the quasi-analytical algorithm (QAA) for estimating total absorption coefficient of turbid inland waters in northeast China," *IEEE J. Sel. Topics Appl. Earth Observ. Remote Sens.*, vol. 9, no. 9, Sep. 2016, Art. no. 4022.
- [42] I. D. Joshi and E. J. D'Sa, "An estuarine-tuned quasi-analytical algorithm (QAA-V): Assessment and application to satellite estimates of SPM in Galveston bay following hurricane harvey," *Biogeosciences*, vol. 15, 2018, Art. no. 4065.
- [43] H. Bernini, H. D. Borges, and J. Martinez, "Quasi-Analytical algorithm calibration for retrieval of inherent optical properties from extremely turbid waters: The case of Madeira river basin," in *Proc. IEEE Int. Geosci. Remote Sens. Symp.*, 2019, pp. 6150–6153.
- [44] K. Shi, Y. Zhang, X. Liu, M. Wang, and B. Qin, "Remote sensing of diffuse attenuation coefficient of photosynthetically active radiation in lake Taihu using MERIS data," *Remote Sens. Environ.*, vol. 140, pp. 365–377, 2014.
- [45] T. S. Moore, M. D. Dowell, S. Bradt, and A. R. Verdu, "An optical water type framework for selecting and blending retrievals from bio-optical algorithms in lakes and coastal waters," *Remote Sens. Environ.*, vol. 143, pp. 97–111, 2014.
- [46] M. Wang and W. Shi, "The NIR-SWIR combined atmospheric correction approach for MODIS ocean color data processing," *Opt. Express*, vol. 15, pp. 15722–15733, 2007.
- [47] Z. Mao, J. Chen, D. Pan, B. Tao, and Q. Zhu, "A regional remote sensing algorithm for total suspended matter East China sea," *Remote Sens. Environ.*, vol. 124 pp. 819–831, 2012.
- [48] F. Mélin, "Impact of inter-mission differences and drifts on chlorophyll-a trend estimates," *Int. J. Remote Sens.*, vol. 37, pp. 2061–2079, 2016.
- [49] J. Chen, T. W. Cui, J. Ishizaka, and C. S. Lin, "A neural network model for remote sensing of diffuse attenuation coefficient in global oceanic and coastal waters: Exemplifying the applicability of the model to the coastal regions in eastern China seas," *Remote Sens. Environ.*, vol. 148, pp. 168–177, 2014.
- [50] C. D. Mobley, "Estimation of the remote-sensing reflectance from above-surface measurements," *Appl. Opt.*, vol. 38, no. 36, pp. 7442–7455, 1999.
- [51] C. Hu, Z. Lee, and B. Franz, "Chlorophyll algorithms for oligotrophic oceans: A novel approach based on three-band reflectance difference," *J. Geophysical Res., Oceans*, vol. 117, 2012, Art. no. C01011.
- [52] V. Volpe, S. Silvestri, and M. Marani, "Remote sensing retrieval suspended sediment concentration in shallow waters," *Remote Sens. Environ.*, vol. 115, pp. 44–54, 2011.
- [53] W. Shi, Y. Zhang, and M. Wang, "Deriving total suspended matter concentration from the near-infrared-based inherent optical properties over turbid waters: A case study in lake Taihu," *Remote Sens.*, vol. 10, 2018.
- [54] D. A. Siegel, M. H. Wang, S. Maritorena, and W. Robinson, "Atmospheric correction of satellite ocean color imagery: The black pixel assumption," *Appl. Opt.*, vol. 39, no. 21, pp. 3582–3591, 2000.
- [55] A. Morel and L. Prieur, "Analysis of variances in ocean color," *Limnol. Oceanogr.*, vol. 22, pp. 709–722, 1977.
- [56] F. Mélin, V. Vantrepotte, A. Chuprin, M. Grant, T. Jackson, and S. Sathyendranath, "Assessing the fitness-for-purpose of satellite multi-mission ocean color climate data records: A protocol applied to OC-CCI chlorophyll-a data," *Remote Sens. Environ.*, vol. 203, pp. 139–151, 2017.
- [57] D. Pauly *et al.*, "Towards sustainability world fisheries," *Nature*, vol. 418, pp. 689–689, 2002.
- [58] T. P. Barnett, D. W. Pierce, and R. Schnur, "Detection of anthropogenic climate change in the world's oceans," *Science*, vol. 292, pp. 270–273, 2001.
- [59] S. Bojinski, M. Verstraete, T. C. Peterson, C. Richter, A. Simmons, and M. Zemp, "The concept of essential climate variables in support of climate research, applications, and policy," *Bull. Amer. Meteorological Soc.*, vol. 95, pp. 1431–1443, 2014.